

Mass loss from advective accretion disc around rotating black holes

Ramiz Aktar^{1*}, Santabrata Das¹, Anuj Nandi² *

¹Indian Institute of Technology Guwahati, Guwahati, 781039, India.

²Space Astronomy Group, SSIF/ISITE Campus, ISRO Satellite Centre, Outer Ring Road, Marathahalli, Bangalore 560037, India

Accepted . Received ; in original form

ABSTRACT

We examine the properties of the outflowing matter from an advective accretion disc around a spinning black hole. During accretion, rotating matter experiences centrifugal pressure supported shock transition that effectively produces a virtual barrier around the black hole in the form of post-shock corona (hereafter, PSC). Due to shock compression, PSC becomes hot and dense that eventually deflects a part of the inflowing matter as bipolar outflows because of the presence of extra thermal gradient force. In our approach, we study the outflow properties in terms of the inflow parameters, namely specific energy (\mathcal{E}) and specific angular momentum (λ) considering the realistic outflow geometry around the rotating black holes. We find that spin of the black hole (a_k) plays an important role in deciding the outflow rate $R_{\dot{m}}$ (ratio of mass flux of outflow and inflow), in particular, $R_{\dot{m}}$ is directly correlated with a_k for the same set of inflow parameters. It is found that a large range of the inflow parameters allows global accretion-ejection solutions and the effective area of the parameter space (\mathcal{E} , λ) with and without outflow decreases with black hole spin (a_k). We compute the maximum outflow rate ($R_{\dot{m}}^{max}$) as function of black hole spin (a_k) and observe that $R_{\dot{m}}^{max}$ weakly depends on a_k that lies in the range $\sim 10\% - 18\%$ of the inflow rate for the adiabatic index (γ) with $1.5 \geq \gamma \geq 4/3$. We present the observational implication of our approach while studying the steady/persistent Jet activities based on the accretion states of black holes. We discuss that our formalism seems to have the potential to explain the observed Jet kinetic power for several Galactic Black Hole sources (GBHs) and Active Galactic Nuclei (AGNs).

Key words: accretion, accretion disc - black hole physics - shock waves - ISM: jets and outflows -X-rays: binaries.

1 INTRODUCTION

Powerful Jets and outflows are commonly observed in accreting black hole systems including active galactic nuclei (AGNs) and X-ray binaries (XRBs) (Mirabel *et al.* 1992; Mirabel & Rodriguez 1994; Hjellming & Rupen 1995; Ferrari 1998; Mirabel & Rodriguez 1998; Junor *et al.* 1999; Cheung 2002; Mirabel 2003; Miller *et al.* 2012). In spite of the availability of wealth of high resolution observations, the physical mechanism of Jet generation and its powering processes are still remain unclear. However, the obvious cause seems to be the extreme gravity that powers the outflows where spin of the central objects may play an important role in producing the relativistic Jets. Earlier work of

Penrose (1969) demonstrated that infalling particles on to a rotating black hole have the potential to extract some of the rotational energy of the black holes. Close to the horizon, space-time geometry is dragged due to black hole rotation and the magnetic field lines are twisted resulting the transport of energy from the black hole along the field lines. Blandford & Znajek (1977) showed that this purely electromagnetic energy extraction mechanism via the threading of magnetic field lines has the potential to power the Jets. This appealing mechanism clearly indicates that black hole spin perhaps play an important role to produce Jets in black hole systems. In order to establish this feature observationally, attempts have been made to find the evidence of spin-powered Jets for the stellar mass black holes. According to Steiner *et al.* (2013) and McClintock *et al.* (2014), significant positive correlation between the radio luminosity associated with the mechanical power of ballistic Jets and

* E-mail: ramiz@iitg.ernet.in (RA); sbdas@iitg.ernet.in (SD), anuj@isac.gov.in (AN)

the spin of the black hole is seen when the transient black hole systems are fed at Eddington-limited accretion rates. However, Russell *et al.* (2013) and Fender & Gallo (2014) ruled out the direct evidence of any such correlation between the transient Jet power and the black hole spin. Using radio-optical correlation, van Velzen & Falcke (2013) also reported that the black hole spin possibly does not have any dominant role in powering the Jets. In a numerical endeavor, De Villiers *et al.* (2005) claimed that the Jet efficiency increases by two orders of magnitude for rapidly rotating black hole compared to the non-spinning black hole. In the similar context, Fernández *et al.* (2015) showed that the more mass is evacuated from the disc as the black hole spin is increased. In an early effort, Donea & Biermann (1996) also found that the Jet power is strongly dependent on the spin of the black holes without considering the Jet geometry. Overall, all the above findings are in contrast and therefore, inconclusive.

Meanwhile, some authors pointed out that there exists a confirm connection between the accretion spectral states and the Jet states (i.e., thick and thin) in black hole systems, particularly for microquasars (Gallo *et al.* 2003; Rushton *et al.* 2010). In the *low-hard spectral states (LHS)* of galactic black holes, quasi-steady and persistent Jets are observed whereas relatively stronger Jets are launched generally in the *hard-intermediate state (HIMS)*. In addition, transient relativistic ejections are observed during the state transition from *hard-intermediate to soft-intermediate state (SIMS)* (Fender *et al.* 2004, 2009). Interestingly, Jet activities are not seen in the *high-soft states (HSS)*. It has also been observed that during ejections, Quasi-Periodic Oscillations (QPOs) are not observed and energy spectra get softens (Vadawale *et al.* 2001; Miller-Jones *et al.* 2012; Radhika & Nandi 2014). This is conjectured in a way that the matter is ejected from the inner part of the disc (i.e., Compton corona equivalently PSC) (Feroci *et al.* 1999; Nandi *et al.* 2001a; Chakrabarti *et al.* 2002). Towards this, very recently, Radhika & Nandi (2014) reported the inflow-outflow connection through the observation in *Radio* and *X-ray* bands for the object XTE J1859+226 and claimed that the fast variation of the ‘spectro-temporal’ properties of outbursting GBHs are connected with the disruption of the post-shock disc (i.e., PSC) in terms of evacuation of matter in the form of Jets (Radhika *et al.* 2015). They pointed out that the QPOs are not seen during ‘transient’ ejection of Jets observed in *Radio*. This result indicates that PSC possibly be responsible for the origin of QPOs in GBHs (Chakrabarti & Manickam 2000; Nandi *et al.* 2001a,b). When Jets are emerged out at the cost of the evacuation/disruption of PSC, QPOs are missing (Vadawale *et al.* 2001; Radhika & Nandi 2014). Extensive MHD simulations of accretion disk around rotating black holes also indicate that windy hot materials (i.e., corona) blows away from the inner part of the disc as Jets (Koide *et al.* 2002; McKinney & Gammie 2004; De Villiers *et al.* 2005). Meanwhile, Das *et al.* (2014) showed that PSC modulates quasi-periodically when viscosity parameter is chosen to its critical value and such modulation successfully exhibits quasi-periodic variation of PSC as well as the outflow rates. These scenarios indicate that there seems to be direct correlation between PSC and outflow. Based on these correlations, one can conjecture that the disk-jet symbiosis is strongly coupled and advective ac-

creting disc perhaps be responsible for the launching of Jets and outflows.

Advective accretion flow around the black holes must be transonic in order to satisfy the inner boundary conditions. Inflowing matter experiences a virtual barrier in the vicinity of the black hole due to centrifugal repulsion against gravity. According to the second law of thermodynamics, such a virtual barrier triggers the discontinuous transition of the flow variables in the form of shock wave in order to prefer the high entropy solution when possible (Fukue 1987; Chakrabarti 1989; Lu *et al.* 1999; Becker & Kazanas 2001; Fukumura & Tsuruta 2004). Due to compression, the shock induced accretion flow produces hot and dense post-shock corona (PSC) surrounding the black holes which essentially acts as the effective boundary layer of the black holes. During accretion, a part of the inflowing matter is deflected by PSC which is further driven out in the vertical direction by the excess thermal gradient force across the shock, producing bipolar outflows. Such an appealing mechanism to launch outflow from the vicinity of the black hole has been confirmed through numerical simulations (Molteni *et al.* 1994, 1996; Machida *et al.* 2000; De Villiers *et al.* 2005; Okuda 2014; Das *et al.* 2014; Okuda & Das 2015). In addition, numerous attempts have been made theoretically to calculate the mass outflow rate around black holes. Chakrabarti (1999) calculated the mass outflow rate considering isothermal flow. Using both Keplerian and sub-Keplerian components, Das *et al.* (2001a) self-consistently estimated mass loss from the disc and found that outflow rate strongly depends on both components. Singh & Chakrabarti (2011) implemented the energy dissipation across the shock while obtaining the outflow rate and found that possibility of mass loss anti-correlates with the dissipation rate. Following the work of Molteni *et al.* (1996), several authors (Chattopadhyay & Das 2007; Das & Chattopadhyay 2008; Kumar & Chattopadhyay 2013; Kumar *et al.* 2013; Das *et al.* 2014) studied the properties of mass outflow rate in terms of inflow parameters considering dissipative accretion flow. However, all these works were carried out with limitation as spin of the black hole was not considered.

Motivating with this, we model the inflow-outflow activity around a rotating black hole. Since the PSC is induced by the shock transition itself, we self-consistently calculate the properties of shock driven outflows in terms of the inflow parameters and investigate the effect of the black hole spin on it. For simplicity, we adopt the pseudo-Kerr potential proposed by Chakrabarti & Mondal (2006) to describe the space time geometry around the black hole. This potential accurately reproduces the particle trajectories around rotating black holes having spin $a_k \lesssim 0.8$. We calculate the global accretion solutions in presence of thermally driven outflows and obtain the parameter spaces spanned by energy and angular momentum of the inflowing matter in terms of the black hole spin. We observe that the shock induced global inflow-outflow solutions exist for wide range of inflow parameters. Varying the inflow parameters, we estimate the *maximum mass outflow rate* (R_m^{\max}) as function of black hole spin (a_k) and find that R_m^{\max} weakly depends on a_k having highest value $\sim 17\% - 18\%$ of the inflow rate for $\gamma = 4/3$. Further, we calculate the *unabsorbed X-ray* flux of several

black hole objects using the *RXTE*¹ satellite archival data and obtain their accretion rates considering the accretion efficiency $\eta = 0.3$ (Thorne 1974), which perhaps reasonable for rotating black holes. With this, using our theoretical estimate of maximum mass outflow rate, we then compute the maximum Jet kinetic power (L_{Jet}^{\max}). These results are further compared with those available from observations and close agreements are seen. Following this, our theoretical prediction essentially provides an estimate of L_{Jet}^{\max} for those sources for which observed Jet power is uncertain.

In the next Section, we describe the basic assumptions and the governing equations for our model. In §3, we discuss the methodology to calculate the mass outflow rates self-consistently. In §4, we present the results which is followed by discussions. In §5, we apply our formalism to calculate the Jet kinetic power for several astrophysical objects (GBHs and AGNs). Finally in §6, we draw the concluding remarks.

2 MODEL EQUATIONS AND ASSUMPTIONS

We consider an axisymmetric disc-jet system around a rotating black hole in the steady state. Here, the accretion disc lies along the black hole equatorial plane while the Jet geometry is described about the black hole rotation axis. In this work, we mainly focus on the inner region of the accretion disc, where the viscous time scale is larger than the in-fall time scale and therefore, the angular momentum transport due to the differential motion is weakly significant leaving the flow to be inviscid there (Chakrabarti 1989). Further, in our model, Jets are originated from the inner part of the accretion disc (PSC) with the same angular momentum of the disc as we neglect the effect of resulting torque in the disc-jet system. Next, we present the governing equations that describe the fluid properties of the accretion disc and the Jets. All the equations are written in geometric unit system as $G = M_{BH} = c = 1$, where, G is the Gravitational constant, M_{BH} is the black hole mass and c is the speed of light, respectively. In this system, the unit of length, mass and time are expressed as GM_{BH}/c^2 , M_{BH} and GM_{BH}/c^3 .

2.1 Governing equations for Accretion

We consider a geometrically thin, axisymmetric, low angular momentum, advective accretion flow around a rotating black hole. For simplicity, we adopt the pseudo-Kerr effective potential introduced by Chakrabarti & Mondal (2006) to represent the space-time geometry around the black hole instead of using full general relativistic prescription. This enables us to solve the problem following the Newtonian approach and keeping all the salient features of space-time geometry around it. The equation of motion describing the accreting matter is given by,

(i) the energy conservation equation:

$$\mathcal{E} = \frac{v^2}{2} + \frac{a^2}{\gamma - 1} + \Phi, \quad (1)$$

where, \mathcal{E} represent the specific energy of the flow, v is the

radial velocity and a is the adiabatic sound speed defined as $a = \sqrt{\gamma P/\rho}$. Here, P is the isotropic pressure, ρ is the gas density, γ is the adiabatic index, respectively. The accreting gas is described by the adiabatic equation of state as $P = K\rho^\gamma$, where K is the measure of specific entropy, which is constant except at the shock transition. The effective potential Φ is given by (Chakrabarti & Mondal 2006),

$$\Phi = -\frac{B + \sqrt{B^2 - 4AC}}{2A}, \quad (2)$$

where,

$$A = \frac{\alpha^2 \lambda^2}{2x^2},$$

$$B = -1 + \frac{\alpha^2 \omega \lambda r^2}{x^2} + \frac{2a_k \lambda}{r^2 x},$$

$$C = 1 - \frac{1}{r - x_0} + \frac{2a_k \omega}{x} + \frac{\alpha^2 \omega^2 r^4}{2x^2}.$$

Here, x and r represent the cylindrical and spherical radial distance considering the black hole is located at the origin of the coordinate system and λ is the specific angular momentum of the flow. Here, $x_0 = 0.04 + 0.97a_k + 0.085a_k^2$, $\omega = 2a_k/(x^3 + a_k^2 x + 2a_k^2)$ and $\alpha^2 = (x^2 - 2x + a_k^2)/(x^2 + a_k^2 + 2a_k^2/x)$, α is the redshift factor and a_k represents the black hole rotation parameter defined as the specific spin angular momentum of the black hole. According to Chakrabarti & Mondal (2006), the above potential mimic the Kerr geometry quite satisfactorily for a wide range of $a_k \lesssim 0.8$.

(ii) the mass conservation equation:

$$\dot{M} = 4\pi\rho v x h, \quad (3)$$

where, \dot{M} denotes the mass accretion rate which is constant everywhere except the region of mass loss and h is the half-thickness of the disk obtained from thin disk approximation (Chakrabarti 1989) as,

$$h(x) = a \sqrt{\frac{x}{\gamma \Phi'_r}}, \quad (4)$$

where, $\Phi'_r = (\partial\Phi/\partial r)_{z < x}$, z is the vertical height in the cylindrical coordinate system and $r = \sqrt{x^2 + z^2}$.

Combining the expression of sound speed and the adiabatic equation of the state of the gas, we calculate the entropy accretion rate as (Chakrabarti 1990),

$$\dot{\mathcal{M}} = v a^\nu \sqrt{\frac{x^3}{\gamma \Phi'_r}}, \quad (5)$$

where, $\nu = (\gamma + 1)/(\gamma - 1)$. In an accretion disk, $\dot{\mathcal{M}}$ remain constant all throughout except at the shock transition where local turbulence generates entropy. Therefore, the entropy accretion rate in the post-shock region is higher than that in the pre-shock region.

By definition, the accretion flow around the black holes must be transonic in nature. This is due to the fact that the velocity of the accreting matter at large distances from the

¹ <http://www.heasarc.gsfc.nasa.gov>

black hole is negligibly small and therefore, the flow is subsonic. However, flow crosses the event horizon with velocity equivalent to the speed of light implying that the flow is supersonic close to the black hole. This clearly indicates that the accretion flow necessarily changes its sonic state during its journey from the outer edge of the disc to the horizon. In order to calculate the location where the state of this sonic transition occurs, we derive the sonic point conditions using Eqs. (1-5) and obtain as,

$$\frac{dv}{dx} = \frac{N}{D}, \quad (6)$$

where,

$$N = \frac{a^2}{\gamma + 1} \left[\frac{3}{x} - \frac{d \ln \Phi'_r}{dx} \right] - \frac{d \Phi_e}{dx}, \quad (7)$$

and

$$D = v - \frac{2a^2}{(\gamma + 1)v}, \quad (8)$$

where, the subscript ‘e’ signifies the quantity measured at the disc equatorial plane. Since the accretion flow is smooth everywhere, the radial velocity gradient must be finite everywhere too. According to Eq. (6), if the denominator D vanishes at any radial distance, the numerator N also vanishes there. Such a location, where $D = N = 0$, is called as sonic point. Setting $D = 0$ and $N = 0$ independently, we find the sonic point conditions as,

$$D = 0 \Rightarrow M_c = \frac{v_c}{a_c} = \sqrt{\frac{2}{\gamma + 1}}, \quad (9)$$

and

$$N = 0 \Rightarrow a_c^2 = (\gamma + 1) \left(\frac{d \Phi_e}{dx} \right)_c \left[\frac{3}{x} - \frac{d \ln \Phi'_r}{dx} \right]_c^{-1}. \quad (10)$$

Here, the subscript ‘c’ denotes the quantities evaluated at the sonic points. We use sonic point conditions, namely, Eqs. (9-10), in Eq. (1) to obtain the location of sonic point for a given set of (\mathcal{E}, λ) of the flow. For a physically acceptable transonic solution, flow must contain at least one saddle type sonic point (Das (2007) and references therein). Depending on the values of \mathcal{E} and λ , flow may possess multiple sonic points as well which is one of the necessary condition to form a shock wave (Chakrabarti 1990). At the sonic point, Eq. (6) takes the form as $dv/dr = 0/0$ and therefore, we use l’Hospital rule to calculate the radial velocity gradient there. Once the flow variables at the sonic point are known, we integrate Eq. (6) starting from the sonic point inward up to the black hole horizon and outward to a large distance to obtain the full set of global accretion solution which may own standing shock waves.

2.2 Governing equations for Outflow

In this work, we consider the outflow to be emerged out from the accretion disc along the rotation axis of the black hole with the same energy and angular momentum as the accretion flow since we neglect the dissipative processes (i.e., viscosity, cooling etc.). Similar to accretion flow, we consider the outflow to obey the polytropic equation of state as $P_j =$

$K_j \rho_j^\gamma$, where, the suffix ‘j’ denotes the outflow variables. The equations of motion that describe the outflow dynamics are given by,

(i) *the energy conservation equation of outflow:*

$$\mathcal{E}_j = \frac{1}{2} v_j^2 + \frac{a_j^2}{\gamma - 1} + \Phi, \quad (11)$$

where \mathcal{E}_j ($\equiv \mathcal{E}$) represent the specific energy of the outflow, v_j is the outflow velocity and a_j is the sound speed of the outflow, respectively.

(ii) *Mass conservation equation of outflow:*

$$\dot{M}_{out} = \rho_j v_j \mathcal{A}, \quad (12)$$

where, \mathcal{A} is a geometrical quantity representing the total area function of the outflow. To obtain \mathcal{A} , we consider the outflow geometry as described in Molteni *et al.* (1996) where the outflowing matter tends to come out through the two surfaces, namely the centrifugal barrier (CB) and the funnel wall (FW). We calculate the centrifugal barrier by identifying the pressure maxima surface as $(d\Phi/dx)_{r_{CB}} = 0$ and the funnel wall by defining the null effective potential as $\Phi|_{r_{FW}} = 0$ (Molteni *et al.* 1996). As the effective potential of our interest is complex in nature, it is unattainable to prevail an analytical expression of the CB surface and the FW and therefore, we compute them numerically. In Figure 1, we illustrate the outflow geometry around the rotating black holes for a wide range of a_k marked in the figure and compare them with the same obtained using the pseudo-Newtonian potential introduced by Paczyński & Wiita (1980) appropriate for a stationary black hole. The regions bounded by the dashed and dotted curves are for $a_k = -0.998$ and $a_k = 0.8$, respectively and the solid curves depict the result of stationary black hole. Note that the outflow geometry for stationary as well as for rotating black holes is indistinguishable outside the range of few tens of Schwarzschild radius. This is possibly due to the fact that the effect of black hole spin on the space-time geometry cursorily diminishes with the increasing distances. Keeping this in mind, we therefore adopt the outflow geometry of the stationary black hole for our present study in order to avoid the rigorous numerical calculations. This enables us to obtain an analytical expression of area function \mathcal{A} and its higher order derivatives, which is required in the sonic point analysis of outflowing matter (Das & Chattopadhyay 2008). A comprehensive study of sonic point analysis for outflows including the area function \mathcal{A} and its derivatives have already been presented in Das & Chattopadhyay (2008) and therefore, we avoid repetition here.

3 SOLUTION METHODOLOGY

In this study, we consider the post-shock matter (PSC) as the precursor of the Jet base and thus, we focus only to those accretion solutions that possess standing shock waves. For shock, the accretion flow variables experience discontinuous transition characterized by the Rankine-Hugoniot (hereafter R-H) shock conditions (Landau & Lifshitz 1959). These conditions include the conservations of mass flux, energy flux

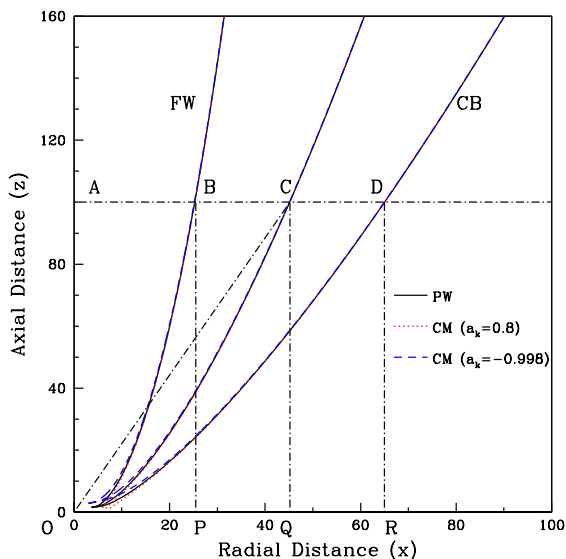


Figure 1. Comparison of Jet geometry for angular momentum $\lambda = 3.3$. Funnel wall (FW) and centrifugal barrier (CB) are marked in the figure. Here, $OC = r_j$ is the spherical radius representing the streamline of the outflow. Dashed and dotted are obtained for $a_k = -0.998$ and 0.8 while solid curve denotes the result obtained using pseudo-Newtonian potential (Paczynski & Wiita 1980). Jet geometries for stationary as well as rotating black holes are indistinguishable beyond few tens of Schwarzschild radius. See text for details.

and momentum flux across the shock, respectively. In presence of mass loss, a part of the inflowing matter is effectively emerged out as outflow from the post-shock region (PSC), while the remaining matter is advected in to the black hole straight away. Therefore, in the present scenario, the shock conditions are given by,

(i) *Conservation of mass flux:*

$$\dot{M}_+ = \dot{M}_- - \dot{M}_{out} = \dot{M}_-(1 - R_{\dot{m}}). \quad (13a)$$

The quantities having subscripts ‘-’ and ‘+’ are referred to the values before and after the shock which we follow throughout the paper unless otherwise stated. The pre-shock and post-shock accretion rates are denoted by \dot{M}_- and \dot{M}_+ , respectively and \dot{M}_{out} is the mass flux for the outflowing matter. Following this, the mass outflow rate is computed as $R_{\dot{m}} = \dot{M}_{out}/\dot{M}_-$. The next condition is

(ii) *Conservation of energy flux:*

$$\mathcal{E}_+ = \mathcal{E}_-, \quad (13b)$$

and finally, we have

(iii) *Conservation of momentum flux:*

$$W_+ + \Sigma_+ v_+^2 = W_- + \Sigma_- v_-^2, \quad (13c)$$

where, W and Σ represent the vertically integrated pressure and density (Das *et al.* 2001b).

We rewrite Eq. (13b) and Eq. (13c) in terms of Mach number ($M = v/a$) and are given by,

$$\frac{1}{2}M_+^2 a_+^2 + \frac{a_+^2}{\gamma - 1} = \frac{1}{2}M_-^2 a_-^2 + \frac{a_-^2}{\gamma - 1} \quad (13d)$$

and

$$\left[\frac{2a_+}{(3\gamma - 1)M_+} + M_+ a_+ \right] = \frac{1}{1 - R_{\dot{m}}} \left[\frac{2a_-}{(3\gamma - 1)M_-} + M_- a_- \right], \quad (13e)$$

where we utilize Eq. (13a) and $a = \sqrt{(3\gamma - 1)W/(2\Sigma)}$ (Das *et al.* 2001b).

Using Eqs. (13d-e), we obtain a shock invariant quantity (C_s) in terms of Mach number M as,

$$C_s = \frac{\left[\frac{2}{M_+} + (3\gamma - 1)M_+ \right]^2 (1 - R_{\dot{m}})^2}{[2 + (\gamma - 1)M_+^2]} = \frac{\left[\frac{2}{M_-} + (3\gamma - 1)M_- \right]^2}{[2 + (\gamma - 1)M_-^2]},$$

where, M_- and M_+ stand for Mach number just before and after the shock in the pre-shock and post-shock flow, respectively.

Since the shock conditions are coupled with inflow and outflow variables, the accretion and Jet equations are solved simultaneously. We obtain the Jet velocity gradient from its governing equations and calculate the sonic point properties following the ‘critical point’ analysis (Chakrabarti 1989). While doing this, we use the inflow parameters, namely, energy \mathcal{E} and angular momentum λ of the inflow. This is because the outflow is considered to be originated from the the post-shock region (PSC). This also ensures that the Jets are launched with the same density as the post-shock flow, namely $\rho_j = \rho_+$. Further, we integrate the Jet equations to calculate the outflow variables at the Jet base starting from the Jet sonic point and using Eqs. (3), (4) and (12) we compute the mass outflow rate in terms of the inflow-outflow properties at the shock and is given by,

$$R_{\dot{m}} = \frac{\dot{M}_{out}}{\dot{M}_-} = \frac{\rho_j v_j(x_s) \mathcal{A}(x_s)}{4\pi \rho_- v_- x_s h_-} = \frac{R v_j(x_s) \mathcal{A}(x_s)}{4\pi \sqrt{\frac{1}{\gamma} x_s^{3/2} \Phi_r'^{-1/2} a_+ v_-}}, \quad (14)$$

where, $R = \Sigma_+/\Sigma_-$ ($\equiv \rho_+ h_+/\rho_- h_- = \rho_+ a_+/\rho_- a_-$), is the compression ratio and $v_j(x_s)$ and $\mathcal{A}(x_s)$ are the Jet velocity and the Jet area function at the shock, respectively. We utilize an iterative method to calculate $R_{\dot{m}}$ self-consistently which is given as follows:

We begin with $R_{\dot{m}} = 0$. Using the shock invariant quantity, we calculate the virtual shock location x_s^v for a given set of (\mathcal{E} , λ) with the consideration that the entropy of the inflowing post-shock matter (\dot{M}_+) and outflowing matter (\dot{M}_{out}) are larger than the entropy of the pre-shock matter (\dot{M}_-). This eventually reflects the fact of second law of thermodynamics as the shocked solutions ascertain the preferred mode of accretion. We use the same set of inflow parameters for Jet equations and calculate $R_{\dot{m}}$ which we employ further in the shock invariant equation to obtain a new shock location. We continue this iteration process until the solution converges to the actual shock location and accordingly we compute the corresponding $R_{\dot{m}}$. In the following Sections, we investigate the properties of x_s and $R_{\dot{m}}$ in terms of the inflow parameters (\mathcal{E} , λ) for various values of black hole spin (a_k) and present the results which are followed by the discussion on astrophysical applications.

4 RESULTS AND DISCUSSIONS

In an advective accretion process around black holes, the accreting matter suffers discontinuous shock transitions due to

the centrifugal barrier. This causes the post-shock flow to become hot and puffed up which eventually behaves like an effective boundary layer around the black hole (i.e., PSC). During accretion, a part of the inflowing matter is deflected vertically by this boundary layer to produce thermally driven outflows. To illustrate the complete picture of the accretion and ejection mechanism, we present the global inflow-outflow solutions for various a_k in Fig. 2. In panel (a), (b) and (c), we show the variation of Mach number ($M = v/a$) of the inflow with the radial distance (x) for $a_k = 0.8$, 0.0, and -0.998 , respectively. Subsonic matter at large distance gradually gains its radial velocity as it proceeds towards the black hole due to the fatal attraction of gravity and crosses the outer sonic point (x_{out}) to become supersonic as shown by the arrows. As the flow continues its journey further towards the black hole, it experiences discontinuous transition in flow variables when the R-H conditions are favorable which is indicated by the dashed vertical arrow. After this transition, flow momentarily slows down and gradually picks up its velocity. Eventually, flow becomes supersonic again after crossing the inner sonic point (x_{in}) and finally enters into the black hole. As the outflow is emerged out from the effective boundary layer of the black hole, the density of the post-shock flow is decreased causing the reduction of pressure at PSC as well. In order to maintain the pressure balance across the standing shock in presence of mass loss, shock itself has to move inward which is indicated by the solid vertical arrow. In the panel (d), we plot the Mach number (M_j) variation of the outflowing matter with its radial coordinate (x_j) corresponding to panel (a), (b) and (c). The black solid circles represent the sonic locations and the arrows show the direction of motion of the outflowing matter. The inflow parameters for panel (a) is $(\mathcal{E}, \lambda) = (0.007, 2.65)$, for (b) is $(0.0025, 3.45)$ and for (c) is $(0.0015, 4.0)$, respectively.

In Fig. 3, we compare the location of the shock transitions as function of energy \mathcal{E} for a set of angular momentum λ . In the upper panel, we choose $a_k = 0.6$ and find that the inflow-outflow solution possesses shock wave for a wide range of \mathcal{E} and λ . As anticipated in Fig. 2, the shock location moves towards to the black hole horizon when $R_{\dot{m}} \neq 0$ just to maintain the pressure balance across the shock. We again observe that the shock location reaches to its lowest value around $x_s^{\min} \sim 8r_g$ at energies higher compared to the case of $R_{\dot{m}} = 0$ and the limiting value of this energy increases with the decrease of angular momentum of the flow. However, the maximum value of energy that allows shock transition in presence of mass loss is identical with no mass loss case. This provides a clear hint that the range of inflow parameters for outflows, namely energy \mathcal{E} and angular momentum λ are reduced from their lower ends. In the lower panel, we consider $a_k = -0.6$ and obtained the similar results which differ only quantitatively. Overall, it is clear that the possibility of shock formation is affected substantially due to the presence of outflow.

Before we proceed further, we now investigate the effect of the black hole rotation on the generation of mass outflow rate. In Fig. 4, we present the variation of shock location (x_s) and outflow rate ($R_{\dot{m}}$) as function of a_k . Here, we fix $\mathcal{E} = 0.002$ and vary λ from 2.8 to 3.92 from the right most curve to the left most with an interval $\Delta\lambda = 0.16$. In the upper panel, the solid curves represent the shock locations

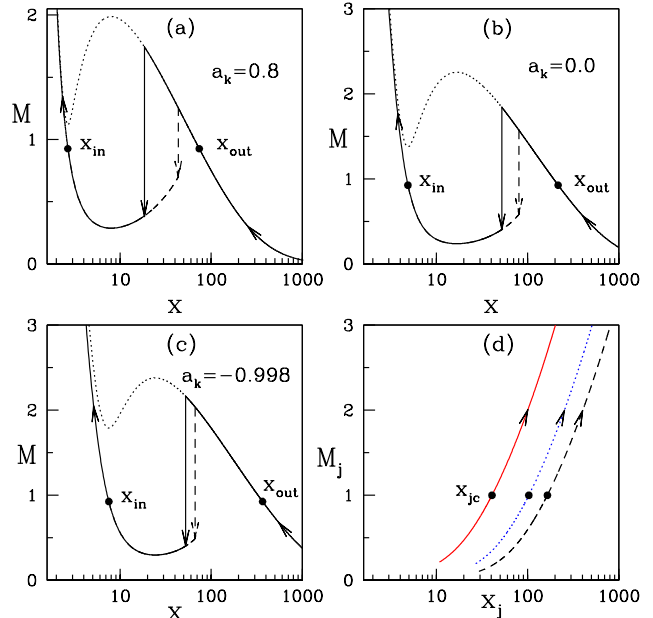


Figure 2. Variation of the inflowing Mach number M ($= v/a$) with radial distances (x) for (a) $a_k = 0.8$, (b) $a_k = 0$ and (c) $a_k = -0.998$, respectively. The corresponding outflow Mach number M_j ($= v_j/a_j$) variation is shown in panel (d). See text for details.

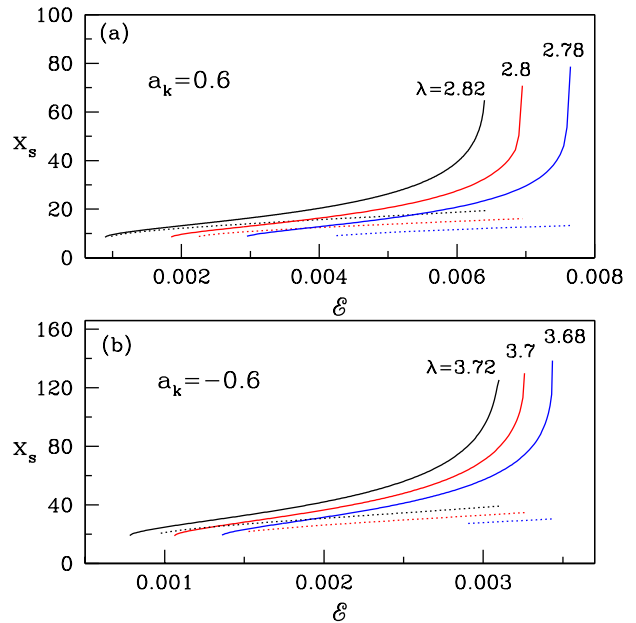


Figure 3. Variation of shock location as function of energy \mathcal{E} . The solid curves represent results without mass loss and the dotted curves are with mass loss. In the upper panel, we choose $a_k = 0.6$ and curves are for $\lambda = 2.78$ (right), 2.80 (middle) and 2.82 (left), respectively. In the lower panel, we consider $a_k = -0.6$ and curves are for $\lambda = 3.68$ (right), 3.70 (middle) and 3.72 (left), respectively.

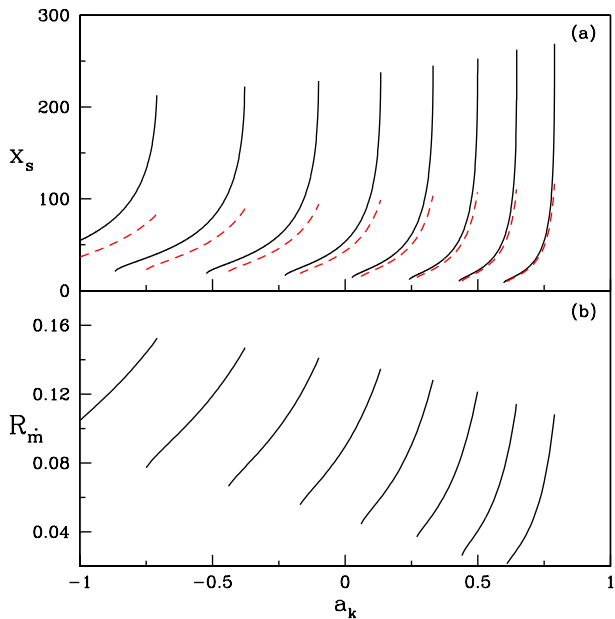


Figure 4. Variation of (a) shock location (x_s) and (b) outflow rate (R_m) as function of black hole rotation parameter a_k for $\lambda = 2.8$ to 3.92 (right to left), where $\Delta\lambda = 0.16$. Here, we fixed the flow energy as $\mathcal{E} = 0.002$. In the upper panel, dashed curves denotes the variation of shock location in presence of outflow.

in absence of mass loss. However, in presence of mass loss, accretion flow adjusts the location of the shock transition closer to the black hole horizon in a way that the pressure balance condition across the shock is maintained which is depicted by the dashed curves. On the contrary, as a_k is increased for a set of \mathcal{E} and λ , the shock locations recede away from the black hole horizon. This indicates that the size of the post-shock region (PSC) is enhanced with the increase of a_k and the inflowing matter is eventually intercepted by the large effective area of the post-shock flow that produces more outflow rate. In the lower panel, we present the feature of outflow rate variation with a_k . For a set of \mathcal{E} and λ , the outflow rate R_m shows non-linear correlation for prograde as well as retrograde flows. In addition, we observe that for a given a_k , R_m is higher for increasing λ and with this, we infer that large outflow rate is associated with the higher λ and lower a_k when \mathcal{E} is fixed. Overall, we find that outflow rate reaches close to 16% for these parameters as depicted in the figure.

Next, we study the characteristics of the post-shock quantities in terms of the inflow variables and present them in Fig. 5. Here, we choose the angular momentum as $\lambda = 2.8$ and vary energy \mathcal{E} and black hole rotation parameter a_k . In the upper panel, we plot the variation of shock location (x_s) with \mathcal{E} for a_k varied from 0.6 (right) to 0.8 (left) with $\Delta a_k = 0.05$. The corresponding variation of outflow rate R_m is shown in the middle panel. Due to shock transition, the post-shock flow is compressed. The measure of this compression is quantified as the ratio of the post-shock density to the pre-shock density and it is termed as shock compression ratio R . In the lower panel, we present the variation of R with \mathcal{E} . When shock forms closer to the black hole horizon,

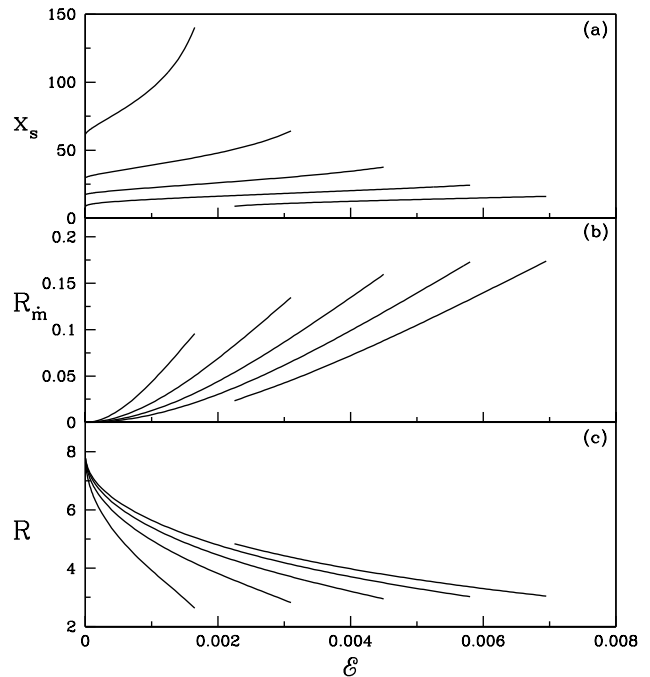


Figure 5. Variation of (a) shock location (x_s), (b) outflow rate (R_m) and (c) compression ratio (R) as function of energy \mathcal{E} for $a_k = 0.6, 0.65, 0.7, 0.75$ and 0.8 (right to left). Here, we fix the flow angular momentum $\lambda = 2.8$.

the amount of gravitational potential energy release is higher ensuing the formation of strong shock. As the energy is increased, the shock location moves outward that increases the outflow rate and weakens the shock compression ratio. We observe similar behaviour for all a_k . However, for a given λ and a_k , there is a range of energy beyond which mass outflow ceases to exist. This provides an indication of finding a parameter space for shock in the fundamental plane of energy and angular momentum of the inflow. We perform the similar study for retrograde flow as well and find the identical trend as depicted in Fig. 6.

As we pointed out earlier that the transonic accretion solutions including R-H shock waves are not isolated solutions. In fact, these solutions do exist for a wide range of parameters, namely, energy (\mathcal{E}), angular momentum (λ), and black hole rotation parameter (a_k). Towards this, we identify the shock induced global accretion solutions using the parameter space spanned by the energy (\mathcal{E}) and angular momentum (λ) of the flow and classify them in terms of a_k . In Fig. 7, we separate the parameter spaces with the solid boundaries that indicate the regions for global shock accretion solutions in absence of mass loss. The corresponding values of a_k are marked in the figure. We further investigate the parameter spaces that cater mass loss and indicate it with the dashed boundaries. Due to mass loss, the post-shock region (PSC) shrinks as seen in Fig. 2, and therefore, the associated parameter space is reduced compared to the results having no outflows, particularly towards the lower energy and lower angular momentum sides (see Fig. 3). For flows with input parameters chosen from these part of the parameter space, shock forms very close to the black hole horizon when outflow is ignored (Das *et al.* 2001b) and they

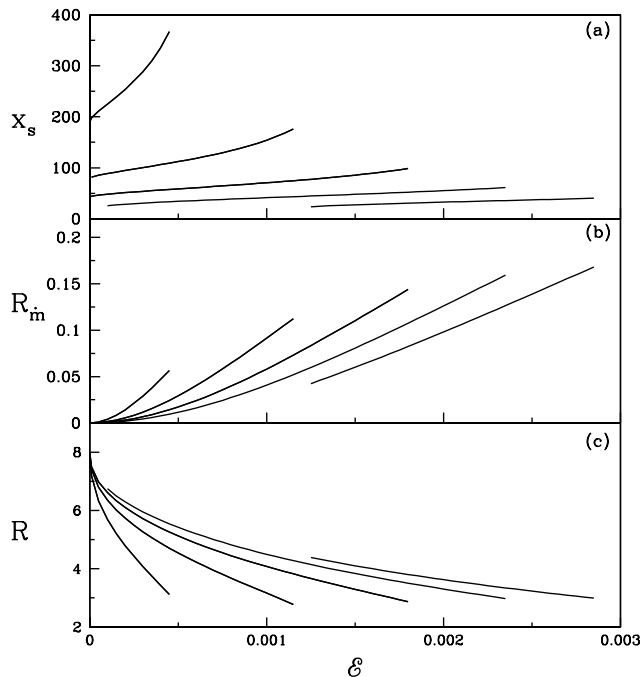


Figure 6. Same as Fig. 5. Here, $a_k = -0.998, -0.8, -0.6, -0.4,$ and -0.2 (right to left) and flow angular momentum is $\lambda = 3.9$.

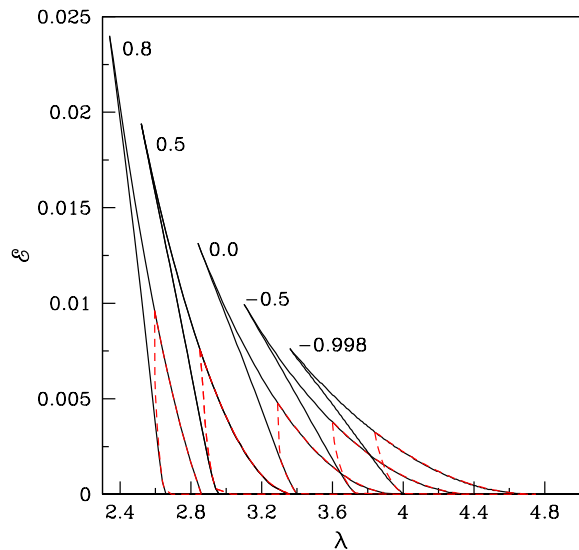


Figure 7. Energy angular momentum parameter space. Solid curve (black): shock parameter space without outflow. Dashed curve (red): shock parameter space with outflow. Various values of a_k are marked in the figure.

cease to exist when the outflow is allowed to emerge out from the post-shock disc.

So far, we have presented the shock induced complete global inflow-outflow solutions and its properties for a given value of $\gamma = 4/3$. In reality, however, the theoretical limit of γ lies in the range between $4/3$ to $5/3$ depending on the ratio between the thermal energy and the rest energy

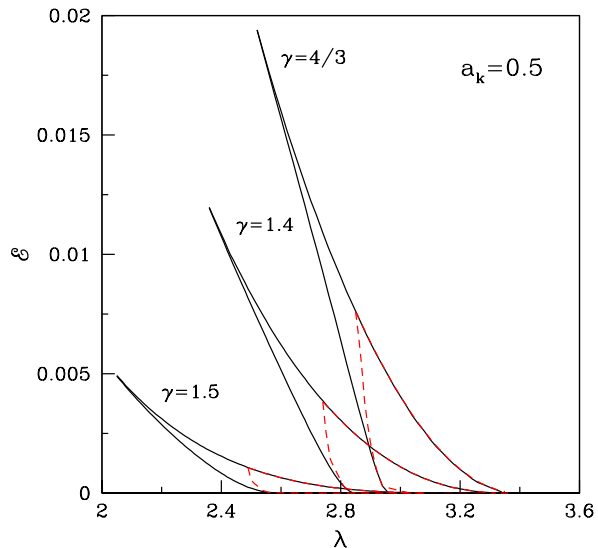


Figure 8. Effective regions of parameter space separated in terms of shock waves transition for various values of γ marked in the figure. Here, we choose $a_k = 0.5$. The solid boundary denotes the presence of shock waves in absence of mass loss and the dashed boundary represents the results including mass loss.

of the flow (Frank *et al.* 2002). To infer this, we consider rotating flows that are characterized as thermally ultra-relativistic ($\gamma \sim 4/3$), thermally trans-relativistic ($\gamma \sim 1.4$) and thermally semi-non-relativistic ($\gamma \sim 1.5$), respectively (Kumar *et al.* 2013) and obtain the parameter spaces for $a_k = 0.5$ similar to Fig. 7. This is shown in Fig. 8. Here, we observe that in all three cases shocks exist for significant range of inflow parameters. However, the range of parameters for shock reduces considerably as the flow changes its ultra-relativistic character towards the non-relativistic limit. In addition, we find that all the parameter spaces further shrink as in Fig. 7, when a part of the inflowing matter is deflected in the form of mass loss from the inner part of the disc (PSC).

According to the formalism adopted in this work, the mass outflow rate $R_{\dot{m}}$ is computed self-consistently in terms of the inflow parameters around a black hole of rotation parameter a_k . This allows us to estimate the maximum $R_{\dot{m}}^{max}$ for a given value of γ . While doing this, we identify a particular set of energy (\mathcal{E}) and angular momentum (λ) from their full range that provides the highest value of $R_{\dot{m}}$. The importance of this investigation is associated with the study of the maximum Jet kinetic power corresponding to $R_{\dot{m}}^{max}$, which we discuss in the next section. Following Fig. 8, we calculate the variation of $R_{\dot{m}}^{max}$ as function of a_k for various values of γ which is presented in Fig. 9. The results displayed in upper, middle and bottom panels are for $\gamma = 4/3, 1.4$ and 1.5 , respectively. We find that $R_{\dot{m}}^{max}$ gradually increase with the increase of a_k for all cases. We also observe that the accretion flows having $\gamma = 4/3$ have the potential to produce more outflows compared to the flows with higher values of γ . This is perhaps inevitable due to the fact that the outflows under consideration are thermally driven and therefore, thermally ultra-relativistic flows exhibit max-

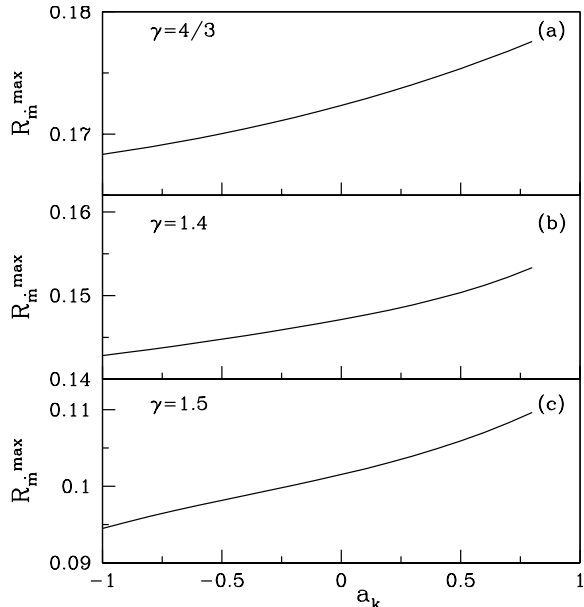


Figure 9. Variation of maximum outflow rates R_m^{\max} with the black hole rotation parameter a_k . Upper panel is for $\gamma = 4/3$ (a), middle panel is for $\gamma = 1.4$ (b) and bottom panel is for $\gamma = 1.5$ (c), respectively. See text for details.

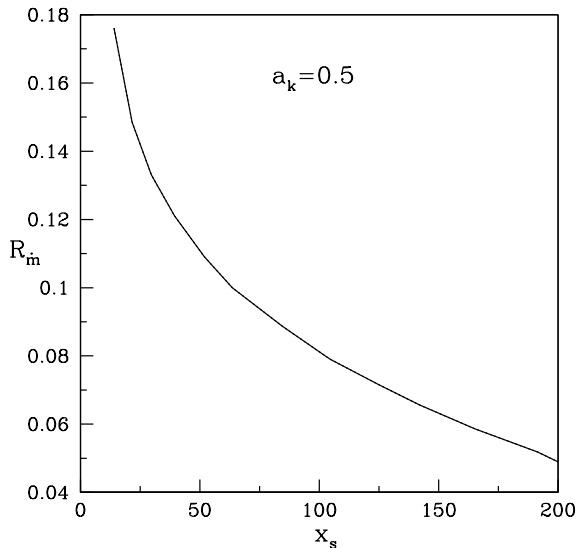


Figure 10. Variation of outflow rate (R_m) with shock location (x_s) obtained for different sets of energy (\mathcal{E}) and angular momentum (λ). Here, $a_k = 0.5$ is used for representation. See text for details.

imum outflows. Following this, in the next Section, we consider $\gamma = 4/3$ while computing the Jet kinetic power for GBHs and AGNs, until otherwise stated.

Until now, we discuss the various properties of the accretion-ejection solutions in terms of the inflow parameters. However, all these studies are based on the assumption of stationary state that does not represent the dynamical behaviour of accretion flows around the outbursting BH sources. Usually, these sources change their accre-

tion states with time and the characteristic features of the emergent radiations and the Jet properties are also varied accordingly. During these dynamical change of states, it is unlikely that the dissipative properties (i.e., viscosity, cooling processes etc.) of the accretion flow will remain constant all throughout, instead, they seem to adjust in a such way that suitably represents the dynamical variation of PSC. In *LHS* of GBHs, the typical geometry of PSC is quite large which reduces considerably in *HIMS* as the dynamical shock moves towards the black hole during the rising phase of the outburst. Such a trend has been reported while modeling the evolution of QPO frequencies for several black hole sources (Chakrabarti *et al.* 2008, 2009; Nandi *et al.* 2012; Debnath *et al.* 2013; Radhika & Nandi 2014; Iyer *et al.* 2015). Interestingly, it is also observed that most of the GBH sources show persistent/steady radio emission during these accretion states (Fender *et al.* 2004, 2009). Now, we attempt to address the evolution of accretion states from *LHS* to *HIMS* and its association with mass loss using our present formalism as case by case which possibly acts as a local model at individual time frame. Toward this, a set of energy and angular momentum (\mathcal{E}, λ) of the inflowing matter is identified which would represent their local values for a dissipative accretion flow and obtain the shock location x_s and outflow rate R_m for a given a_k . Since the post-shock geometry (PSC) is associated with x_s , as anticipated earlier, we chose various such sets of (\mathcal{E}, λ) in a way that x_s moves towards the black hole and show the variation of R_m with x_s in Fig. 10 for a typical value of $a_k = 0.5$. Note that R_m is increased with the decrease of x_s resulting more Jet kinetic power that represents the common characteristic of radio emissions observed in outbursting sources.

5 ASTROPHYSICAL APPLICATION

Here, we attempt to estimate the mass outflow rate and its associated Jet kinetic power for various astrophysical black hole sources (GBHs and AGNs) using our present formalism. Since our work deals with the steady outflows, we focus only to those sources particularly to their accretion states where persistent/steady Jets are observed. These Jets are essentially compact (i.e., optically thick) in nature and are not isolated completely from the core of the central engine (Mirabel & Rodriguez 1994, 1998; Corbel *et al.* 2000, 2001; Fender *et al.* 2001).

5.1 Jet kinetic power predicted from Accretion States

We consider five black hole sources namely, XTE J1859+226, GRO J1655-40, GX 339-4, H 1743-322 and GRS 1915+105, respectively. For these sources, mass (M_{BH}), distance (d) and spin (a_k) are constrained within the accuracy limit and are given in Table 1. In order to estimate the Jet kinetic power, we calculate the X-ray flux for these sources in the *low-hard state (LHS)* and *hard-intermediate state (HIMS)* using *RXTE*¹ satellite data.

In general, GBH sources undergo outbursts (Homan & Belloni 2005; Remillard & McClintock 2006; Debnath *et al.* 2008; Nandi *et al.* 2012; Debnath *et al.* 2013; Radhika & Nandi 2014; Iyer *et al.* 2015) and show activity

of radio emissions coupled with the accretion states of their evolution during the outburst phases (Brocksopp *et al.* 2002; Fender *et al.* 2004, 2009; Cadolle Bel *et al.* 2011; Miller-Jones *et al.* 2012; Radhika & Nandi 2014). It has also been observed that most of the outbursting sources show persistent/steady Jet activity during *LHS* and *HIMS* while transient ‘relativistic’ ejections are observed during the transition from hard-intermediate to soft-intermediate state (Brocksopp *et al.* 2002; Fender *et al.* 2004, 2009; Radhika & Nandi 2014).

In order to estimate the ‘model predicted’ Jet power based on accretion states, we estimated X-ray flux from a single observation of each states (i.e., *LHS* and *HIMS*) for all the sources from different outburst phases (as mentioned in the Table-1). We use archival data obtained from the HEASARC database of the *RXTE* satellite for the estimation of X-ray flux for all the five sources. We extracted and analyzed background-subtracted PCA (3 - 30 keV) spectral data using PCU2 detector (i.e., well calibrated detector) for our specific purpose. The standard FTOOLS package of HEASOFT v6.15.1 was used for spectral data reduction (see Nandi *et al.* (2012); Radhika & Nandi (2014) for details). For spectral analysis and modeling, we used the packages of XSPEC v12.8.1.

We have done spectral modeling for each observations from each spectral states (i.e., *LHS* and *HIMS*) for all the five sources using PCA spectral data in the energy range of 3 - 30 keV. We model the energy spectrum using the phenomenological accretion disk model i.e., consisting of a *diskbb* and a *power-law* component. In this modeling, the *diskbb* and *power-law* components provide the contribution from the accretion disk and ‘hot’ Compton corona (i.e., PSC) and thereby one can estimate the total *unabsorbed* X-ray flux (F_x , in units of $\text{ergs cm}^{-2} \text{s}^{-1}$) emitted from the accretion disk around the GBH sources.

Once we obtain the *unabsorbed* X-ray flux (F_x) of a source, we calculate the X-ray luminosity (L_x) of the source employing the relation $L_x = 4\pi d^2 F_x$, where d is the distance of the source. Assuming the maximum radiative efficiency of the infalling matter around rotating black hole is $\eta \sim 0.3$, we calculate the accretion rate of the black hole as,

$$\dot{M}_{acc} = 2.99 \times 10^{-16} \left(\frac{F_x d^2}{c^2} \right) \left(\frac{M_{BH}}{M_\odot} \right)^{-1} \dot{M}_{Edd}.$$

Here, M_{BH} denotes the mass of the black hole and \dot{M}_{Edd} represents the Eddington accretion rate. Next, we calculate the mass outflow rate using our theoretical estimate (Eq. 14) which has its maximum limit (R_{in}^{\max}) for a particular set of ($a_k, \mathcal{E}, \lambda$) (see Fig. 9). With this, we find the *maximum mass outflow rate* as $\dot{M}_{out} = R_{in}^{\max} \dot{M}_{acc}$ which successively allows us to compute the *maximum Jet kinetic power* as,

$$L_{Jet}^{\max} = R_{in}^{\max} \times \dot{M}_{acc} \times c^2 \text{ ergs s}^{-1}. \quad (15)$$

As pointed out earlier that steady and persistent radio emissions are observed during *LHS* and *HIMS* (Fender *et al.* 2004, 2009). In addition, there are indications that the radio emission increases while the state transition from *LHS* to *HIMS* takes place. Moreover, the radio emission becomes non-steady during the *HIMS* itself just prior to the ejection and it is quite known that the relativistic ejections take place during the transition from *HIMS* to *SIMS* (Fender *et al.* 2004, 2009). All these observations perhaps indicate that

the persistent Jet activity would be maximum during *HIMS*. Therefore, in order to study the outflow properties in the *HIMS*, we consider the maximum outflow rate obtained from our model calculation (see Fig. 9) and use it to estimate the Jet kinetic power. On the other hand, Jet kinetic power in the *LHS* is expected to be lower than the *HIMS* although its quantitative estimate is unclear. Therefore, we use outflow rate to be around $\sim 10\%$ as a representative value while calculating the Jet kinetic power for *LHS*. Below, we mention the fundamental properties of each sources and present the details for the estimation of Jet kinetic power corresponding to individual states of a particular observation.

XTE J1859 + 226:

Filippenko & Chornock (2001) first presented the dynamical estimate of mass of the source to be around $7.4 \pm 1.1 M_\odot$. Recently, Radhika & Nandi (2014) claimed that the mass of XTE J1859 + 226 is perhaps in between $6.58 M_\odot - 8.84 M_\odot$ which is similar to the prediction of Shaposhnikov & Titarchuk (2009) although the lower mass limit is estimated as $5.4 M_\odot$ by Corral-Santana *et al.* (2011). However, we consider the typical mass of the source as $7 M_\odot$. The distance of this source is around $d \sim 11 \text{ kpc}$ (Filippenko & Chornock 2001). Steiner *et al.* (2013) measured the spin as $a_k \sim 0.4$, however, Motta *et al.* (2014a) recently reported the spin of the source is $a_k \sim 0.34$. Since the spin predictions are quite close, we use $a_k \sim 0.4$ for this analysis. We estimate the fluxes F_x (see Table 1) of *LHS* and *HIMS* of the 2009 outburst of the source (Radhika & Nandi 2014). The corresponding disc luminosities are calculated as $L_{disc}^{LHS} = 8.26 \times 10^{37} \text{ ergs s}^{-1}$ and $L_{disc}^{HIMS} = 1.85 \times 10^{38} \text{ ergs s}^{-1}$, respectively. Now, it is reasonable to assume the accretion efficiency for rotating black hole as $\eta = 0.3$ which corresponds to the accretion rate of the inflowing matter as $\dot{M}_{acc}^{LHS} = 0.304 \dot{M}_{Edd}$ in *LHS* and $\dot{M}_{acc}^{HIMS} = 0.680 \dot{M}_{Edd}$ in *HIMS*. For *LHS*, we use $R_{in} = 9.83\%$ following our theoretical estimate where $x_s = 64.6 r_g$ for $a_k = 0.4$, $\mathcal{E} = 0.00198$ and $\lambda = 3.18$. Incorporating these inputs in Eq. (15), we obtain the Jet kinetic power as $L_{Jet}^{LHS} = 2.52 \times 10^{37} \text{ ergs s}^{-1}$. The maximum mass outflow rate for *HIMS* corresponding to $a_k = 0.4$ is obtain from Fig. 9 as $R_{in}^{\max} = 17.5\%$ for $\mathcal{E} = 0.00547$, and $\lambda = 3.1$, where the shock transition occur at $21.9 r_g$. Using these values in Eq. (15), we obtain the maximum Jet kinetic power as $L_{Jet}^{HIMS} = 1.08 \times 10^{38} \text{ ergs s}^{-1}$ which we regard to be associated with the *Hard-Intermediate* state of this source.

GRO J1655-40:

The mass of the source GRO J1655-40 is reported by Greene *et al.* (2001) and is given by $6.3 M_\odot$. Recently, Motta *et al.* (2014b) estimated the object mass as $5.31 \pm 0.07 M_\odot$. This source is located at around $d \sim 3.2 \text{ kpc}$ and the spin of this source is estimated by Shafee *et al.* (2006) using *RXTE*¹ and *ASCA* data through the modeling of the thermal spectral continuum and obtained in the range $a_k \sim 0.65 - 0.75$ (and reference therein). Fitting the strong reflection features of iron line in *XMM-Newton* data, Reis *et al.* (2009) determines the lower limit of the spin of

Table 1. Accretion state dependent Jet kinetic power.

Objects	M_{BH}	d	a_k	Observation (3 – 30 keV)		\dot{M}_{acc}	$R_{\dot{m}}$	L_{Jet}	L_{Jet}^{Obs} #
	(M_{\odot})	(kpc)		States	F_x (ergs cm $^{-2}$ s $^{-1}$)	(\dot{M}_{Edd})*	(%)	(ergs s $^{-1}$)	(ergs s $^{-1}$)
XTE J1859+226 (2009 Outburst)	7	11	0.4	<i>LHS</i>	5.71×10^{-9}	0.304	9.83	2.52×10^{37}	1.82×10^{38} (1)
				<i>HIMS</i>	12.79×10^{-9}	0.680	17.5	1.08×10^{38}	
GRO J1655-40 (2005 Outburst)	6.3	3.2	0.7	<i>LHS</i>	3.19×10^{-9}	0.016	9.98	1.18×10^{36}	3.01×10^{36} (2)
				<i>HIMS</i>	8.02×10^{-9}	0.040	17.68	5.79×10^{36}	
GX 339-4 (2002 Outburst)	7.5	15	0.4	<i>LHS</i>	15.71×10^{-9}	1.450	9.98	1.29×10^{38}	2.92×10^{38} (1)
				<i>HIMS**</i>	12.12×10^{-9}	1.118	17.5	1.90×10^{38}	
H 1743-322 (2009 Outburst)	8	8.5	0.2	<i>HIMS</i>	4.03×10^{-9}	0.112	17.35	2.01×10^{37}	1.08×10^{38} (3)
GRS 1915+105 (1997 Observation)	12.4	8.6	$> 0.98^{\dagger}$	<i>LHS</i>	20.33×10^{-9}	0.373	9.98	5.99×10^{37}	8.06×10^{37} (1)

* $\dot{M}_{Edd} = 1.44 \times 10^{17} \left(\frac{M_{BH}}{M_{\odot}} \right) \text{ gm s}^{-1}$

** Total flux in *HIMS* (3 – 30 keV) is smaller than *LHS* as the contribution of the hard X-ray flux (> 10 keV) in *HIMS* is less.

$L_{Jet}^{Obs} = \eta \dot{M}_{out} c^2$ is used for the source H 1743–322, where \dot{M}_{out} is the outflow rate (see reference). For other sources, $L_{Jet}^{Obs} = L_r \times L_{Edd}$ is used, where L_r is the observed Jet power (in *Edd*) (see references) and $L_{Edd} = 1.3 \times 10^{38} \left(\frac{M_{BH}}{M_{\odot}} \right) \text{ ergs s}^{-1}$.

References: (1) Fender *et al.* (2004) (2) Migliari *et al.* (2007) (3) Miller *et al.* (2012)

this object $a_k = 0.9$. Motta *et al.* (2014b) calculated the spin of the object using X-ray timing method and found as $a_k = 0.290 \pm 0.003$ which is an inconsistent estimate compared to iron line or continuum methods. In our present analysis, however, we consider $a_k = 0.7$. As before, we analyzed the 2005 outburst of GRO J1655-40 to calculate the X-ray fluxes (F_x) for *LHS* and *HIMS* (see Table 1) in the energy range 3 – 30 keV and obtain the corresponding accretion rates $\dot{M}_{acc}^{LHS} = 0.016 \dot{M}_{Edd}$ in *LHS* and $\dot{M}_{acc}^{HIMS} = 0.040 \dot{M}_{Edd}$ in *HIMS*. We use $R_{\dot{m}} = 9.98\%$ in case of *LHS* which is obtained for $a_k = 0.7$, $\mathcal{E} = 0.00258$ and $\lambda = 2.845$ where $x_s = 49.98 r_g$. From these values, we estimate Jet kinetic power in *LHS* as $L_{Jet}^{LHS} = 1.18 \times 10^{36} \text{ ergs s}^{-1}$. For *HIMS*, we estimate of the maximum mass outflow rate for $a_k = 0.7$ (see Fig. 9) as $R_{\dot{m}}^{\max} = 17.68\%$ where $\mathcal{E} = 0.0073$ and $\lambda = 2.715$ with $x_s = 16.73 r_g$. These inputs provide the maximum Jet kinetic power as $L_{Jet}^{HIMS} = 5.79 \times 10^{36} \text{ ergs s}^{-1}$.

GX 339-4:

The mass of the object is estimated as $7.5 \pm 0.8 M_{\odot}$ Chen (2011) and distance $d \sim 15$ kpc by Hynes *et al.* (2004). The issue of spin measurement of this objects is not settled yet as there are conflicting measurements. Analyzing the *XMM-Newton* data set for broad iron line detection, Reis *et al.* (2008) and Miller *et al.* (2008) claimed $a_k = 0.935$ while the disc continuum fitting prefers the lower spin having upper limit of $a_k < 0.9$ (Kolehmainen & Done 2010). However, analyzing the wide-band *Suzaku* spectra, Yamada *et al.* (2009) pointed out $a_k < 0.4$. Being aware of these, we consider a conservative estimate of spin as

$a_k = 0.4$ in our calculation. This source has undergone outburst phases several times during RXTE era. For this analysis, we consider the 2002 outburst spectral data (in the energy band of 3 – 30 keV) for *LHS* and *HIMS*. During May 2 of 2002 outburst, the object was in *LHS* emitting X-ray flux of $F_x^{LHS} = 15.71 \times 10^{-9} \text{ ergs cm}^{-2} \text{ s}^{-1}$ (see Table 1) and the disc luminosity of $L_{disc}^{LHS} = 4.22 \times 10^{38} \text{ ergs s}^{-1}$. Using $\eta = 0.3$, the disc rate is calculated as $\dot{M}_{acc}^{LHS} = 1.450 \dot{M}_{Edd}$. Estimating $R_{\dot{m}} = 9.98\%$ from our model using $\mathcal{E} = 0.00198$ and $\lambda = 3.18$ with $x_s = 64.63 r_g$, we calculate the Jet kinetic power $L_{Jet}^{LHS} = 1.29 \times 10^{38} \text{ ergs s}^{-1}$. On May 12 of the 2002 outburst, the source was in *HIMS* and the radiated X-ray flux was calculated as $F_x^{HIMS} = 12.12 \times 10^{-9} \text{ ergs cm}^{-2} \text{ s}^{-1}$ (see Table 1) and the disc luminosity of $L_{disc}^{HIMS} = 3.26 \times 10^{38} \text{ ergs s}^{-1}$. Using $\eta = 0.3$, the disc rate is calculated as $\dot{M}_{acc}^{HIMS} = 1.118 \dot{M}_{Edd}$. Estimating $R_{\dot{m}}^{\max} = 17.5\%$ from our model using $\mathcal{E} = 0.00547$ and $\lambda = 3.1$ with $x_s = 21.9 r_g$, we calculate the maximum Jet kinetic power $L_{Jet}^{HIMS} = 1.90 \times 10^{38} \text{ ergs s}^{-1}$.

H 1743-322:

Miller *et al.* (2012) and Steiner *et al.* (2012) reported the mass, distance and spin of H 1743-322 as $\sim 8 M_{\odot}$, $d \sim 8.5$ kpc and $a_k = 0.2$, respectively. Using the RXTE observation of the 2009 outburst of the source, the disc luminosity for this source is computed for the energy range of 3 – 30 keV corresponding to the measured X-ray flux of $F_x^{HIMS} = 4.03 \times 10^{-9} \text{ ergs cm}^{-2} \text{ s}^{-1}$ in *HIMS* (see Table-1) (Miller-Jones *et al.* 2012) as $4.63 \times 10^{37} \text{ ergs s}^{-1}$. Assuming $\eta = 0.3$, we obtain the accretion rate as $\dot{M}_{acc}^{HIMS} =$

$0.112\dot{M}_{Edd}$. Accretion rate in *LHS* is not known due to lack of observation during the 2009 outburst (Miller-Jones *et al.* 2012). For $a_k = 0.2$, $\mathcal{E} = 0.00485$ and $\lambda = 3.176$, we obtain the maximum mass outflow rate for *HIMS* as $R_{\dot{m}}^{\max} = 17.35\%$ with $x_s = 23.66r_g$. Employing these values, we find the maximum Jet kinetic power as $L_{Jet}^{HIMS} = 2.01 \times 10^{37}$ ergs s^{-1} .

GRS 1915+105:

Earlier, Greiner *et al.* (2001) estimated the mass of GRS 1915+105 as $(14 \pm 4) M_{\odot}$. Recently, Hurley *et al.* (2013) reported the new mass estimate as $(12.9 \pm 2.4) M_{\odot}$ which is further revised as $(12.4 \pm 2) M_{\odot}$ by Reid *et al.* (2014). The distance of the source is reported as $d \sim (9.4 \pm 0.2)$ kpc by Hurley *et al.* (2013) and Reid *et al.* (2014) claimed the distance to be $d \sim (8.6 \pm 2)$ kpc. However, in this calculation we use the mass and distance of the source as $12.4M_{\odot}$ and 8.6 kpc, respectively in order to compute the disc luminosity. The source is extremely rotating as McClintock *et al.* (2006) estimated the spin parameter $a_k > 0.98$ which is similar to the estimate of Blum *et al.* (2009). As the source is highly variable in X-rays, we choose one observation when the source was in the *hard state* that is similar to *LHS* of other GBH sources. *RXTE* observed the source in the energy range of 3 – 30 keV on 22th October, 1997 and object was in so-called χ -class (Belloni *et al.* 2001; Nandi *et al.* 2001c). For this observation, the disc luminosity corresponding to the X-ray flux of $F_x^{LHS} = 20.33 \times 10^{-9}$ ergs $cm^{-2} s^{-1}$ (see Table 1) is obtained as 1.79×10^{38} ergs s^{-1} which provides the disc accretion rate as $\dot{M}_{in}^{LHS} = 0.373\dot{M}_{Edd}$. According to our model, the mass outflow rate for *LHS* (or simply hard state for this source) is calculated as $R_{\dot{m}} = 9.98\%$ where, $x_s = 50.47r_g$ with $a_k = 0.98$, $\mathcal{E} = 0.00276$ and $\lambda = 2.679$. Here, we cross the upper limit of a_k (indicated by dagger (\dagger) in column 4 of Table 1) as the adopted black hole potential satisfactorily describes the space-time geometry for $a_k \lesssim 0.8$. However, we anticipate that the obtained $R_{\dot{m}}$ provides qualitative estimate that would not differ significantly from its exact value. Using these values, the Jet kinetic power is found to be $L_{Jet}^{LHS} = 5.99 \times 10^{37}$ ergs s^{-1} .

In this Section, we calculated the Jet kinetic power mostly for outbursting GBH sources (except GRS 1915+105) for different accretion states (i.e., *LHS* and *HIMS*). Our findings clearly show that as the sources transit from *LHS* to *HIMS*, there is significant increase in the Jet kinetic power. The predicted Jet kinetic powers are in close agreement with the observed values for XTE J1859+226, GRO J1655-40, GX 339-4, GRS 1915+105 and H 1743-322 (Fender *et al.* 2004; Migliari *et al.* 2007; Miller *et al.* 2012).

5.2 Jet kinetic power estimated from Accretion Rates

We further extend our study to estimate the Jet kinetic power for other GBH and AGN sources where we do not observe fast (\sim day scale) state transitions similar to outbursting GBH sources (except XTE J1550-564). In order to calculate the Jet kinetic power for these sources, we find their mass (M_{BH}), accretion rate (\dot{M}_{acc}) and spin (a_k) from the existing literature. Meanwhile, we compute $R_{\dot{m}}^{\max}$

corresponding to black hole spin a_k using our theoretical approach. We then use the values of \dot{M}_{acc} and $R_{\dot{m}}^{\max}$ in Eq. (15) to estimate the Jet kinetic power.

In Table 2, we display the physical parameters of the sources (GBHs and AGNs) under consideration along with the computed Jet kinetic power obtained from our analysis. In column 1-4, we present the list of sources, their mass (M_{BH}), accretion rate (\dot{M}_{in}) and spin (a_k). In column 5-6, we mention the representative values of energy \mathcal{E} , angular momentum λ of the inflow that provide the shock location x_s (in column 7) and the corresponding *maximum mass outflow rate* $R_{\dot{m}}^{\max}$ (in column 8). Finally, in column 9, we present the maximum Jet kinetic power L_{Jet}^{\max} . The first seven sources are GBHs whereas the last three sources are AGNs. Here, we give emphasis on the maximum $R_{\dot{m}}$ in order to speculate the upper limit of Jet kinetic power. We find that the estimated Jet kinetic powers are in close agreement with the observed values at least for few sources, namely Cyg X-1, XTE J1550-564, M87 and Sgr A* (Fender *et al.* 2004; de Gasperin *et al.* 2012; Falcke & Biermann 1999). For remaining sources, we argue that the present method illustrates the typical estimates of Jet kinetic power that possibly lie within the acceptable range. Further, in our analysis, we choose four sources having black hole spin $a_k > 0.8$ which are indicated by dagger (\dagger) in column 4. As before, we anticipate that the obtained L_{Jet}^{\max} for these sources provide qualitative estimates that would not differ significantly from their observed values.

6 CONCLUDING REMARKS

In this work, we self-consistently examine the accretion-ejection mechanism around the rotating black holes. We consider the structure of the accretion disc to be stationary, thin, rotating and advection dominated which contains R-H shock waves. These shocks are formed as a consequence of centrifugal barrier located near the black hole horizon. Based on the second law of thermodynamics, we argue that the shock solutions are dynamically preferred over the smooth solutions as they possess higher entropy (Becker & Kazanas 2001). During accretion, a part of the super-sonic matter is deflected at the centrifugal barrier due to excess thermal pressure caused by the shock compression and eventually emerge out in the form of thermally driven outflows. These outflows are further channeled through the confined geometry bounded by the funnel wall and pressure maxima surface along the rotation axis of the black hole (Molteni *et al.* 1996).

We find that mass loss can occur for prograde as well as retrograde flows. When outflow is emerged out from the inner part of the disk (PSC), post-shock pressure is decreased that essentially compels the shock front to move forward towards the horizon in order to maintain the pressure balance across the shock. Therefore, a flow originally containing shock wave close to its minimum location (x_s^{\min}) for $R_{\dot{m}} = 0$, will not provide any outflow as R-H shock conditions are not favorable there (see Fig. 3). This certainly tells us that the outflow solutions would be restricted compared to the global shocked accretion solutions in absence of mass loss. However, we show that the shock induced global inflow-outflow solutions are not isolated solutions, but ex-

Table 2. Estimated Jet kinetic power from accretion rate.

Objects	M_{BH} (M_{\odot})	\dot{M}_{acc} (\dot{M}_{Edd})	a_k	\mathcal{E} (c^2)	λ (cr_g)	x_s (r_g)	$R_{\dot{m}}^{\max}$ (%)	L_{Jet}^{\max} (ergs s $^{-1}$)	L_{Jet}^{Obs} # (ergs s $^{-1}$)
A0620-00	6.60 (a)	1.684 (b)	0.12 (b)	0.00444	3.25	26.84	17.25	2.48×10^{38}	...
LMC X-3	6.98 (c)	2.487 (d)	0.25 (e)	0.00476	3.15	25.72	17.35	3.90×10^{38}	...
XTE J1550-564	9.10 (f)	0.511 (g)	0.34 (g)	0.00530	3.06	22.07	17.43	1.05×10^{38}	3.55×10^{38} (y)
M33 X-7	15.66 (h)	0.718 (i)	0.84 † (j)	0.00807	2.61	15.60	17.79	2.59×10^{38}	...
4U 1543-47	9.40 (k)	1.315 (l)	0.43 (l)	0.00565	2.98	21.07	17.48	2.80×10^{37}	...
LMC X-1	10.90 (m)	0.853 (n)	0.92 † (n)	0.00830	2.58	15.42	17.93	2.16×10^{37}	...
Cyg X-1	14.80 (o)	0.061 (p)	$\geq 0.95^{\dagger}$ (p)	0.00835	2.58	15.38	17.98	2.10×10^{37}	3.85×10^{37} (y)
Mrk 79	5.24×10^7 (q)	9.82×10^{-2} (r)	0.70 (s)	0.00730	2.72	16.73	17.68	1.18×10^{44}	...
M87	3.50×10^9 (t)	1.16×10^{-4} (u)	≥ 0.65 (v)	0.00705	2.76	16.94	17.62	9.25×10^{42}	1.00×10^{45} (z)
Sgr A*	4.90×10^6 (w)	7.89×10^{-5} (x)	0.99 † (w)	0.00859	2.57	14.71	18.09	9.07×10^{39}	1.00×10^{39} (zz)

$L_{Jet}^{Obs} = L_r \times L_{Edd}$, where L_r is the observed Jet power (in *Edd*) (see references).

References: (a) Cantrell *et al.* (2010) (b) Gou *et al.* (2010) (c) Orosz *et al.* (2014) (d) Kubota *et al.* (2010) (e) Steiner *et al.* (2014) (f) Orosz *et al.* (2011a) (g) Steiner *et al.* (2011) (h) Orosz *et al.* (2007) (i) Liu *et al.* (2008) (j) Liu *et al.* (2010) (k) Orosz (2003) (l) Morningstar & Miller (2014) (m) Orosz *et al.* (2009) (n) Gou *et al.* (2009) (o) Orosz *et al.* (2011b) (p) Gou *et al.* (2011) (q) Peterson *et al.* (2004) (r) Riffel *et al.* (2013) (s) Gallo *et al.* (2011) (t) Walsh *et al.* (2013) (u) Kuo *et al.* (2014) (v) Wang *et al.* (2008) (w) Aschenbach *et al.* (2010) (x) Yuan *et al.* (2002) (y) Fender *et al.* (2004) (z) de Gasperin *et al.* (2012) (zz) Falcke & Biermann (1999)

ist for a wide range of inflow parameters, namely, \mathcal{E} and λ , respectively. Interestingly, numerical simulations also indicate the similar findings as reported by Das *et al.* (2014). We examine the existence of such solutions with and without outflow and obtain the parameter space spanned by the \mathcal{E} and λ as function of black hole rotation parameter a_k . As anticipated above, the parameter space that provides mass outflow is shrunk compared to the case of no outflow (see Fig. 7). In other words, a significant region of the parameter space that exhibits stationary shock for $R_{\dot{m}} = 0$ does not provide steady shock solutions in presence of outflow. This possibly infer that the accreting matter having \mathcal{E} and λ from this region of the parameter space may demonstrate the non-steady behavior (Das *et al.* 2001b; Das 2007) which is triggered simply due to the presence of mass loss. Investigation of such scenario requires time-dependent calculations which is beyond the scope of the present work and we wish to report this elsewhere.

In this work, we mainly focused on thermally ultra-relativistic flows with adiabatic index $\gamma = 4/3$. However, when the cooling effects are negligible, the purely non-relativistic flow behaves like gas-pressure dominated with $\gamma \sim 5/3$. In reality, the value of γ would be an intermediate value depending on the dissipation processes active in the flow. Keeping this in mind, we calculate the parameter space for different values of γ and find that shock forms in all the cases even in presence of outflow. Interestingly, we observe that the effective region of the parameter space is reduced with the increase of γ indicating the limited possibility of shock transition when the flow changes its character towards the non-relativistic regime.

We have estimated the mass outflow rate using the in-

flow parameters, such as, \mathcal{E} and λ . We show that $R_{\dot{m}}$ increases with a_k for a fixed \mathcal{E} and λ (see Fig. 4). This is possibly due to the fact that as a_k is increased shock forms away from the black hole. Therefore, the effective area of the post-shock flow (PSC), where the inflowing matter deflects to generate outflow, becomes large and results enhanced outflow rate. Further, we attempt to find the maximum mass loss ($R_{\dot{m}}^{\max}$) from the disc and quantify it in terms of the inflow parameters. For this, we fix the value of γ and explore all possible combinations of energy and angular momentum to obtain $R_{\dot{m}}^{\max}$. In Fig. 9, we show the variation of $R_{\dot{m}}^{\max}$ with a_k and observe that flow with $\gamma = 4/3$ exhibits the highest outflow rate $R_{\dot{m}}^{\max}$ that lies in the range around $\sim 17\% - 18\%$. Also, very weak correlation is seen between $R_{\dot{m}}^{\max}$ and a_k in all the cases. Moreover, we have shown in Fig. 10 that for various sets of (\mathcal{E}, λ) , $R_{\dot{m}}$ increases with the decrease of x_s (equivalently Jet power increases as the size of the PSC is reduced) based on the realistic scenario (i.e., spectral states transit from *LHS* to *HIMS*) which seems to be a common characteristic observed in GBH sources.

We employ our formalism in order to estimate the Jet kinetic power (L_{Jet}) of several black hole sources (GBHs and AGNs). To begin with, we consider outbursting sources to calculate L_{Jet} based on the accretion states. For these sources, we compute their *unabsorbed* X-ray fluxes in *LHS* and *HIMS* using the data of *RXTE* observation and obtain their disc rate considering the accretion efficiency $\eta = 0.3$ which seems to be relevant for rotating black holes. Then, we calculate the outflow rate using our formalism and employ it in Eq. (15) along with the disc rate to obtain L_{Jet} . While estimating the Jet kinetic power, we consider maximum outflow rate $R_{\dot{m}}^{\max}$ for *HIMS* (see Fig. 9) and $R_{\dot{m}} \sim 10\%$ for

LHS, as discussed in Section 5. In Table 1, we summarize the physical parameters of five black hole sources along with the computed Jet kinetic power. In the process of estimating L_{Jet}^{max} , two quantities play major role. First one is the unabsorbed X-ray flux computed from *RXTE* archival data and the other is the maximum outflow rate obtained from our model calculation. We find that the estimated L_{Jet}^{max} for various sources are in close agreement with the observed values (Fender *et al.* 2004; Miller *et al.* 2012). We further extend our study for other black hole sources where the fast accretion state transitions (\sim day scale) are not seen (except XTE J1550-564). For these sources, the disc rate is obtained from the existing literature (see Table 2) and R_m^{max} is computed from our theoretical calculation which finally provides the L_{Jet}^{max} . We present these results in Table 2. We notice that estimated L_{Jet}^{max} for Cyg X-1, XTE J1550-564, M87 and Sgr A* are also in close agreement with the observed values (Fender *et al.* 2004; de Gasperin *et al.* 2012; Falcke & Biermann 1999). Following this findings, we argue that L_{Jet}^{max} for rest of the sources would also in turn render the representative values which are expected to be consistent with their actual estimates.

The present work has limitations as it is developed based on some approximations. We use pseudo-Kerr gravitational potential to mimic the general relativistic effect around rotating black hole that allows us to examine the properties of non-linear shock solutions in presence of mass loss in a simpler way. We ignore the effect of viscosity and radiative processes. We consider constant adiabatic index instead of calculating it self-consistently based on its thermal properties. Needless to mention that we have not address the issue of transient relativistic ejections and its collimation mechanism as we consider the Jet geometry only up to its sonic point. Although the implementation of all such issues are beyond the scope of this paper, however, we believe that the above approximations will not alter our basic conclusions qualitatively.

ACKNOWLEDGMENTS

We thank the reviewer for suggestions and comments that help us to improve the manuscript. We would like to thank Indranil Chattopadhyay and Samir Mandal for discussions. This research has made use of the data obtained through High Energy Astrophysics Science Archive Research Center on-line service, provided by NASA/Goddard Space Flight Center. AN acknowledges Group Director, SAG, Deputy Director, CDA and Director, ISAC, for continuous support to carry out this research at ISAC, Bangalore.

REFERENCES

Aschenbach B., 2010, Mem. S.A.It, 81, 319
 Becker P. A., Kazanas D., 2001, ApJ, 546, 429
 Belloni T., Méndez M., Sánchez-Fernández C., 2001, A&A, 372, 551
 Blandford R. D., Znajek R. I., 1977, MNRAS, 179, 433
 Blum J. L., *et al.*, 2009, ApJ, 706, 60
 Brocksopp C., *et al.*, 2002, MNRAS, 331, 765
 Cadolle Bel M., *et al.*, 2011, A&A, 534, 119

Cantrell Andrew G., *et al.*, 2010, ApJ, 710, 1127
 Chakrabarti S. K., 1989, ApJ, 347, 365
 Chakrabarti S. K., 1990, Theory of Transonic Astrophysical Flows (Singapore: World Sci.)
 Chakrabarti S. K., 1999, A&A, 351, 185
 Chakrabarti S. K., Manickam S., 2000, ApJ, 531, 41
 Chakrabarti S. K., *et al.*, 2002, ApJ, 579, 21
 Chakrabarti S. K., Mondal S., 2006, MNRAS, 369, 976
 Chakrabarti S. K., *et al.*, 2008, A&A, 489, 41
 Chakrabarti S. K., Dutta B, G., Pal P. S., 2009, MNRAS, 394, 1463
 Chattopadhyay I., Das S., 2007, New Astron., 12, 454
 Chen T, 2011, in Romero G., Sunyaev R., Bellon T., eds, Proc. IAU Symp. 275, Jets at All Scales. Cambridge Univ. Press, Cambridge, p. 327
 Cheung C. C., 2002, ApJ, 581, 15
 Corbel S., *et al.*, 2000, A&A, 359, 251
 Corbel S., *et al.*, 2001, ApJ, 554, 43
 Corral-Santana J. M., *et al.*, 2011, MNRAS, 413, 15
 Das S., *et al.*, 2001a, A&A, 379, 683
 Das S., Chattopadhyay I., Chakrabarti S. K., 2001b, ApJ, 557, 983
 Das S., 2007, MNRAS, 376, 1659
 Das S., Chattopadhyay, I., 2008, New Astron., 549, 556
 Das S., *et al.*, 2014, MNRAS, 442, 251
 Debnath D., *et al.*, 2008, BASI, 36, 151
 Debnath D., Chakrabarti S. K., Nandi A., 2013, AdSpR, 52, 2143
 de Gasperin F., *et al.*, 2012, A&A, 547, 56
 De Villiers, J. P., *et al.*, 2005, ApJ, 620, 878
 Donea A. C., Biermann P. L., 1996, A&A, 316, 43
 Falcke H., Biermann P. L., 1999, A&A, 342, 49
 Fender R. P., *et al.*, 2001, MNRAS, 322, 23
 Fender R. P., Belloni T., Gallo E., 2004, MNRAS, 355, 1105
 Fender R. P., Homan J., Belloni T., 2009, MNRAS, 396, 1307
 Fender R. P., Gallo E., 2014, Space Sci. Rev., 183, 323
 Fernández R., *et al.*, 2015, MNRAS, 446, 750
 Ferrari A., 1998, ARA&A, 36, 539
 Feroci M., *et al.*, 1999, A&A, 351, 985
 Filippenko A. V., Chornock R., 2001, IAU Circular, 7644, 2
 Frank I., King A. R., Raine D., 2002, Accretion power in Astrophysics (Cambridge)
 Fukue J., 1987, PASJ, 39, 309
 Fukumura K., Tsuruta S., 2004, ApJ, 611, 964
 Gallo E., Fender R. P., Pooley G. G., 2003, MNRAS, 344, 60
 Gallo L. C., *et al.*, 2011, MNRAS, 411, 607
 Greene J., Bailyn C. D., Orosz J. A., 2001, ApJ, 554, 1290
 Gou L., *et al.*, 2009, ApJ, 701, 1076
 Gou L., *et al.*, 2010, ApJL, 718, 122
 Gou L., *et al.*, 2011, ApJ, 742, 85
 Greiner J., Cuby J. G., McCaughrean M. J., 2001, Nature, 414, 522
 Hjellming R. M., Rupen M. P., 1995, Nature, 375, 464
 Homan J., Belloni T., 2005, Ap&SS, 300, 107
 Hurley D. J., *et al.*, 2013, MNRAS, 430, 1832
 Hynes R. I., *et al.*, 2004, ApJ, 609, 317
 Iyer N., Nandi A., Mandal S., 2015, ApJ, 807, 108
 Junor W., Biretta J. A., Livio M., 1999, Nature, 401, 891
 Koide S., *et al.*, 2002, Science, 295, 1688

- Kolehmainen M., Done C., 2010, MNRAS, 406, 2206
 Kubota A., *et al.*, 2010, ApJ, 714, 860
 Kumar R., Chattopadhyay I., 2013, MNRAS, 430, 386
 Kumar R., *et al.*, 2013, MNRAS, 436, 2864
 Kuo C. Y., *et al.*, 2014, ApJ, 783, 33
 Landau L. D., Lifshitz, E. D., 1959, Fluid Mechanics (New York: Pergamon)
 Liu J., *et al.*, 2008, ApJ, 679, 37
 Liu J., *et al.*, 2010, ApJ, 719, 109
 Lu J. F., Gu W. M., Yuan F., 1999, ApJ, 523, 340
 Machida M., Hayashi M. R., Matsumoto R., 2000, ApJ, 532, 67
 McClintock J. E., *et al.*, 2006, ApJ, 652, 518
 McClintock J. E., Narayan R., Steiner J., 2014, Space Sci. Rev., 183, 295
 McKinney J. C., Gammie C. F., 2004, ApJ, 611, 977
 Migliari A., *et al.*, 2007, ApJ, 670, 610
 Miller J. M., *et al.* 2008, ApJ, 679, 113
 Miller J. M., *et al.* 2012, ApJL, 759, 6
 Mirabel I. F., *et al.*, 1992, Nature, 358, 215
 Mirabel I. F., Rodriguez L. F., 1994, Nature, 371, 46
 Mirabel I. F., Rodriguez L. F., 1998, Nature, 392, 673
 Mirabel I. F., 2003, New A Rev., 47, 471
 Miller-Jones J. C. A., *et al.*, 2012, MNRAS, 421, 468
 Morningstar W. R., Miller J. M., 2014, ApJ, 793, 33
 Motta S. E., *et al.*, 2014a, MNRAS, 439, 65
 Motta S. E., *et al.*, 2014b, MNRAS, 437, 2554
 Molteni D., Lanzafame G., Chakrabarti S. K., 1994, ApJ, 425, 161
 Molteni D., Ryu D., Chakrabarti S. K., 1996, ApJ, 470, 460
 Nandi A., *et al.*, 2001a, A&A, 380, 245
 Nandi A., *et al.*, 2001b, MNRAS, 324, 267
 Nandi A., Manickam S. G., Chakrabarti S. K., 2001c, IJP, 74(B), 5 (arXiv:astro-ph/0012523)
 Nandi A., *et al.*, 2012, A&A, 542, 56
 Okuda T., 2014, MNRAS, 441, 2354
 Okuda T., Das S., 2015, MNRAS, (in press), DOI: 10.1093/mnras/stv1626
 Orosz J. A., 2003, Proceedings IAU Symposium, 212, A Massive Star Odyssey, from Main Sequence to Supernova, ed. K. A. van der Hucht & C. Esteban (Cambridge: Cambridge Univ. Press), 365
 Orosz J. A., *et al.*, 2007, Nature, 449, 872
 Orosz J. A., *et al.*, 2009, ApJ, 697, 573
 Orosz J. A., *et al.*, 2011a, ApJ, 730, 75
 Orosz J. A., *et al.*, 2011b, ApJ, 742, 84
 Orosz J. A., *et al.*, 2014, ApJ, 794, 154
 Paczyński B., Wiita P., 1980, A&A, 88, 23
 Penrose R., 1969, Nuovo Cimento Rivista Serie, 1, 252
 Peterson B. M., *et al.*, 2004, ApJ, 613, 682
 Radhika D., Nandi A., 2014, AdSpR, 54, 1678
 Radhika D., Nandi A., Seetha S., 2015, in preparation
 Reid M. J., *et al.*, 2014, ApJ, 796, 2
 Reis R. C., *et al.*, 2008, MNRAS, 387, 1489
 Reis R. C., *et al.*, 2009, MNRAS, 395, 1257
 Remillard R. A., McClintock J. E., 2006, ARA&A, 44, 49
 Riffel R. A., Storchi-Bergmann T., Winge C., 2013, MNRAS, 430, 2249
 Rushton A., *et al.*, 2010, A&A, 524, 29
 Russell D. M., Gallo, E., Fender, R. P., 2013, MNRAS, 431, 405
 Shafee R., *et al.*, 2006, ApJL, 636, 113
 Shaposhnikov N., Titarchuk L., 2009, ApJ, 699, 453
 Singh C. B., Chakrabarti S. K., 2011, MNRAS, 410, 2414.
 Steiner J. F., *et al.*, 2011, MNRAS, 416, 941
 Steiner J. F., *et al.*, 2012, ApJ, 745, 7
 Steiner J. F., McClintock J. E., Narayan R., 2013, ApJ, 762, 104
 Steiner J. F., *et al.*, 2014, ApJ, 793, 29
 Thorne K. S., 1974, ApJ, 191, 507
 Vadawale S. V., *et al.*, 2001, A&A, 370, 17
 van Velzen, S., Falcke H., 2013, A&A, 557, L7
 Walsh J. L., *et al.*, 2013, ApJ, 770, 86
 Wang J. M., *et al.*, 2008, ApJ, 676, 109
 Yamada S., *et al.*, 2009, ApJ, 707, L109
 Yuan F., Markoff S., Falcke H., 2002, A&A, 383, 854